DOI: 10.26599/FSHW.2026.9251234

Contents lists available at SciOpen

Food Science and Human Wellness

journal homepage: https://www.sciopen.com/journal/2097-0765

China Food Publishing Co.

Heat-treating FM with Clamshell Powder Ameliorate Postmenopausal Osteoporosis by Regulating Bone-Fat Metabolism.

Hui Yu [a,b,1], Shengliang Yuan [c,1], Yuxiang Feng [a,1], Yudan Mei [a], Hengjun Du [f], Samad Tavakoli [b], Jiayi Shen [a], Menghua Wu [e], Kefeng Wu [a,b,d,*], Hang Xiao [f,*] and Hui Luo [a,b,*]

[a] *Guangdong Medical University, Zhanjiang, 524023, China.*

[b] *Marine Biomedical Research Institute, Guangdong Medical University, Zhanjiang 524023, China.*

[c] *Affiliated Gaozhou People's Hospital, Guangdong Medical University, Gaozhou 525200, China*

[d] *Guangdong Key Laboratory for Research and Development of Natural Drugs, Guangdong Medical University, Zhanjiang, Guangdong, 524023, China*

[e] *School of Pharmacy, Jinan University, Jinan, 250000, China.*

[f] *Department of Food Science, University of Massachusetts, Amherst, Massachusetts 01003, United States.*

ABSTRACT: Postmenopausal osteoporosis is characterized by a disruptive bone-fat imbalance, yet effective therapies remain limited. Here, for the first time, we link the traditional use of fish maw heat-treated with clam shell powder (CPFM) to the restoration of bone-fat balance. Using INFOGEST simulated digestion followed by LC-MS/MS analysis, we found that CPFM peptides were predominantly low-molecular-weight species (84.6% below 1 kDa), with heptapeptides as the most abundant fraction (20%). In ovariectomized mice, CPFM peptides reduced bone marrow fat accumulation and improved bone microstructure (increased BV/TV and BMD). In bone marrow stromal cells (BMSCs), they concurrently inhibited adipogenic differentiation (reduced Oil Red O-positive area) and promoted osteogenesis (enhanced ALP activity and mineralization). From CPFM digests, we systematically screened and identified an absorbable tetrapeptide, FLLL, based on its high relative abundance (37.8%), predicted bioactivity (PeptideRanker >0.5), cell-penetrating ability (CPPpred >0.33), and favorable ADMET properties. In cultured BMSCs, FLLL recapitulated the dual effects of CPFM, promoting osteogenesis while suppressing adipogenesis. Mechanistically, both CPFM and FLLL downregulated adipogenic factors (PPARγ, FABP4, FASN) and upregulated osteogenic markers (RUNX2, COL1α2, BGLAP). Surface plasmon resonance confirmed direct binding of FLLL to RUNX2 (KD = 32.5 μM), and rescue experiments indicated that FLLL regulates the bone-fat balance in association with the PPARγ/RUNX2 axis. Collectively, this study establishes a chain of evidence spanning peptide profiling, *in vivo* efficacy, active component identification, and mechanistic insight. These findings support CPFM as a promising dietary candidate and identify FLLL with well-defined *in vitro* bioactivity.

Keywords: Heat-treated with clamshell powder; Postmenopausal osteoporosis; Peptides; PPARγ; RUNX2

1. Introduction

[1] Hui Yu, Shengliang Yuan and Yuxiang Feng have contributed equally to this work.
***Corresponding author**
winokhere@sina.com (K. Wu), hangxiao@foodsci.umass.edu (H. Xiao), luohui@gdmu.edu.cn (H. Luo).

Received 16 February 2026
Received in revised from 2 May 2026
Accepted 14 July 2026

Postmenopausal osteoporosis (PMOP) is a chronic metabolic bone disease initiated by estrogen decline, leading to bone loss and microstructural deterioration [1]. Estrogen deficiency is frequently associated with obesity [2], creating a vicious cycle that exacerbates bone loss [3]. Pathophysiologically, PMOP involves an imbalance in bone marrow mesenchymal stem cell (BMSC) differentiation within the marrow microenvironment, favoring adipogenesis over osteogenesis and disrupting the bone-fat metabolic axis. Accumulation of bone marrow adipose tissue is a hallmark of PMOP and negatively correlates with bone mineral density. Correcting this local imbalance is therefore a key therapeutic target. Mechanistically, estrogen deficiency upregulates the adipogenic transcription factor peroxisome proliferator-activated receptor gamma (PPARγ), activating downstream effectors such as fatty acid-binding protein-4 (FABP4) and fatty acid synthase (FASN) to drive excessive lipid deposition [4, 5]. Concurrently, elevated PPARγ suppresses the osteogenic master regulator runt-related transcription factor 2 (RUNX2), reducing expression of markers such as bone gamma-carboxyglutamic acid-containing protein (BGLAP) and collagen type I alpha 2 (COL1α2), thereby inhibiting osteogenesis [6]. Current drugs or estrogen therapy primarily target osteoclast inhibition or bone formation, but their efficacy against marrow fat accumulation and the underlying bone-fat metabolic imbalance remains limited [7, 8].

Given these limitations, alternative strategies that target both bone formation and fat accumulation are urgently needed. In recent years, dietary interventions, particularly food-derived bioactive peptides, have gained attention for their dual regulatory potential. Previous studies have shown that food-derived peptides can exert both anti-obesity and anti-osteoporotic effects [9, 10]. Among these, collagen-rich peptides from marine sources have shown particular promise in supporting skeletal health [10]. In contrast, existing pharmacotherapies fail to adequately regulate the bone-fat balance, whereas food-derived peptides demonstrate potential in modulating lipid metabolism and promoting osteogenesis, offering new mechanistic insights. Accordingly, peptide-based nutritional interventions are considered a promising strategy for improving PMOP management.

Among the various sources of bioactive peptides, a traditional Chinese processed product has long been used for bone health. CPFM is prepared by stir-frying fish swim bladder (a collagen-rich tissue) with clam shell powder according to traditional methods. According to the Bencao Gangmu, this processed product is recommended for tonifying the kidney, replenishing essence, and strengthening bones and muscles. The processing method is believed to reduce the greasy nature of the raw material and enhance its medicinal properties [11, 12]. Modern physicochemical studies have shown that the heat treatment facilitates the Maillard reaction, forming stable covalent complexes that improve the stability and bioavailability of peptides [13]. Although previous studies have shown that collagen peptides from fish maw (FM) can promote osteogenesis, their potential adverse effects on lipid metabolism remain a concern. The traditional processing with clam shell powder is thought to mitigate this greasy nature, but systematic in vivo and in vitro evidence that CPFM peptides regulate the bone-fat balance is still lacking. In particular, the absorbable peptides responsible for this effect and their causal mechanisms remain unclear.

To address this gap, we conducted the present study with the following hypothesis: CPFM peptides ameliorate postmenopausal osteoporosis by restoring the bone-fat balance through modulation of the PPARγ/RUNX2 axis, and specific absorbable peptides from CPFM serve as key active components. To identify the absorbable peptides that reach the systemic circulation and potentially exert bioactivity, we first simulated gastrointestinal digestion of CPFM using the INFOGEST protocol and characterized the peptide profile by LC-MS/MS. We then evaluated the effects of CPFM peptide treatment on bone-fat metabolic balance using an ovariectomized (OVX) mouse model, complemented by *in vitro* osteogenic and adipogenic differentiation assays. An integrated proteomic and functional analysis was performed to explore the underlying mechanisms. Finally, through plasma component analysis and bioactivity screening, we identified the tetrapeptide FLLL as a potential active constituent of CPFM peptides. Thus, this study aimed to explore the absorbable bioactive peptides from CPFM and elucidate CPFM peptides mechanism in regulating the bone-fat axis.

2. Method

2.1 Reagents

The manufacturers and batch numbers of the major reagents used in the experiments are listed in Table 1.

Table 1 The major reagents.

No.	Reagents	Manufacturers	Batch number
1	Strontium ranelate	Bailingwei Technology Co., Ltd., Beijing, China	814142
2	Mifobate	Source Leaf Biological Technology Co., Ltd., Shanghai, China	T25404
3	BMSCs-ADM	Procell, Wuhan, China	PD-004
4	BMSCs-ODM	Procell, Wuhan, China	PD-003
5	Estradiol	Abbott Biologicals B.V, IL, USA	373614
6	β-Actin	SAB Biotech, MD, USA	2127
7	Anti-rabbit IgG secondary antibody	SAB Biotech, MD, USA	8715
8	RUNX2	Wuhan Sanying Biotechnology, Wuhan, China	23006218
9	COL1α2	SAB Biotech, MD, USA	5814
10	BGLAP	SAB Biotech, MD, USA	5106
11	FASN	Wuhan Sanying Biotechnology, Wuhan, China	00141632
12	PPARγ	Wuhan Sanying Biotechnology, Wuhan, China	00149915
13	FABP4	Wuhan Sanying Biotechnology, Wuhan, China	00117845

Abbreviations: BMSCs-ADM, mouse bone marrow mesenchymal stem cells adipogenic differentiation medium. BMSCs-ODM, mouse bone marrow mesenchymal stem cells osteogenic differentiation medium. RUNX2, runt-related transcription factor 2; COL1α2, collagen type I alpha 2; BGLAP, bone gamma-carboxyglutamic acid-containing protein; FASN, fatty acid synthase; PPARγ, peroxisome proliferator-activated receptor gamma; FABP4, fatty acid-binding protein 4.

2.2 Preparation of FM and CPFM

FM was procured from *Megalanibea fusca* that were uniformly cultivated, harvested, and air-dried under standardized conditions at Yifanghai Marine Ranch Co., Ltd. (Guangdong, China), as previously described [12]. FM specimens exhibiting consistent texture and size (220-250 g, obtained from 3-year-old fish) were selected. Connective tissue and adipose deposits were carefully dissected and removed, and the

samples were cut into uniform pieces (1 × 1 cm²), rinsed thoroughly with ultrapure water, air-dried, and stored at 25 °C [14].

CPFM was prepared according to an established protocol [12]. Briefly, 30 kg of CP was mixed with 100 kg of dried FM. The mixture was stir-fried at 340 °C with continuous mechanical agitation at 8 rpm for 2 mins, ensuring uniform heating and consistent product quality. The resulting material, designated as CPFM, was allowed to cool to ambient temperature before further use.

2.3 Preparation of CPFM peptides by simulated gastrointestinal digestion

The CPFM peptides were prepared using a simulated gastrointestinal digestion model, as outlined in Fig. 1. The process was adapted from the standardized INFOGEST protocol with modifications [15]. Briefly, ground samples were first hydrated in ultra-pure water (1:10, w/v) at 24°C for 12 h and then heated at 100°C for 2 h. The resulting mixture was lysed in radio immunoprecipitation assay lysis buffer (Beyotime, China) at a ratio of 1:12.5 (g/mL). Subsequent simulated gastric digests were performed at pH 3.0 with artificial gastric fluid (Leagene Biotechnology, China) in a 1:1 (v/v) ratio for 2 h at 37°C, followed by heat inactivation (100°C, 10 min). Similarly, the intestinal phase was conducted at pH 7.0 with artificial intestinal fluid (Leagene Biotechnology, China) under identical conditions (1:1 v/v, 37°C, 2 h) and terminated by heat inactivation. The final hydrolysates were centrifuged, and the supernatants were collected, lyophilized, and stored for LC-MS/MS analysis.

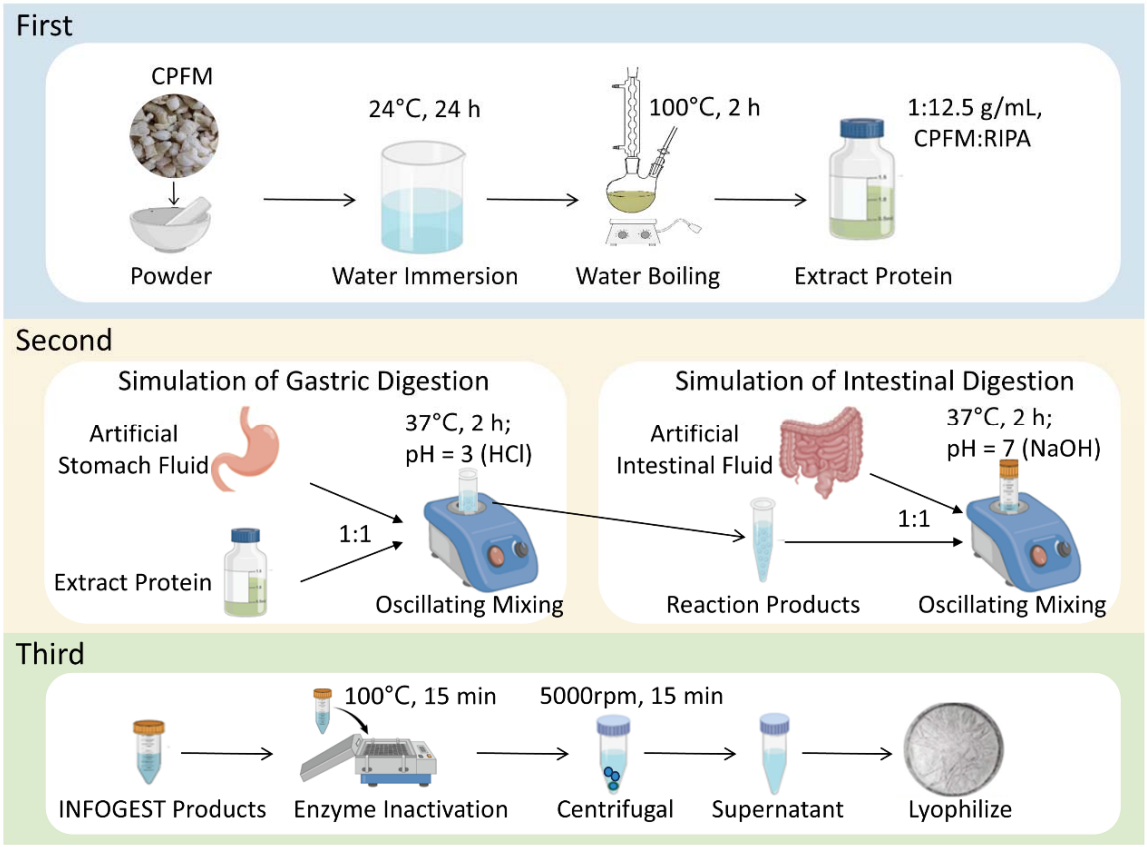

Fig. 1. Schematic diagram of the preparative workflow for CPFM peptides. The process involved three major stages: (First) Preparation of protein extracts via grinding and heat treatment, (Second) Sequential Digestion using the INFOGEST 2.0 protocol, (Third) Termination & Collection of bioactive peptides through heat inactivation, centrifugation, and lyophilization.

2.4 LC-MS/MS analysis for proteins and peptides identification

The protein composition of CPFM, as well as the peptide profiles of their gastrointestinal digests, were characterized by LC-MS/MS. All analyses were performed by Bio-Tech Pack Technology Co. Ltd. (Beijing, China). The samples were first dissolved in 50 mM NH_4HCO_3, reduced with dithiothreitol at 56°C for 1 h, and alkylated with iodoacetamide in the dark for 40 min. The resulting mixture was desalted using a self-packed column and concentrated by vacuum centrifugation at 45°C. LC-MS/MS analysis was conducted on an Orbitrap Fusion Lumos mass spectrometer (Thermo Fisher Scientific) coupled with an Acclaim PepMap C_{18} column (1.5 mm i.d. × 150 mm, 3 μm). The mobile phase consisted of (A) 0.1% formic acid in water and (B) 80% acetonitrile containing 0.1% formic acid. The column temperature was maintained at 20°C.

The chromatographic gradients were as follows: protein analysis (300 nL/min): 5% B (0-2 min), 5→14% B (2-10 min), 14→24% B (10-17 min), 24→34% B (17-23 min), 34→45% B (23-24 min), 45→95% B (24-33 min), and held at 95% B (33-38 min). Peptide analysis (600 nL/min): 4% B (0-2 min), 4→8% B (2-45 min), 8→28% B (45-55 min), 28→40% B (55-56 min), 40→95% B (56-66 min), and held at 95% B (66-71 min).

2.5 Data-independent acquisition (DIA) based proteomics

According to previous report, the eluted peptides were directly injected into a Q Exactive HF-X mass spectrometer (Q Exactive HF-X Hybrid Quadrupole-Orbitrap™ Mass spectrometer, Thermo Fisher Scientific, Rockwell, IL, United States) for DIA [16]. The mass spectrometry method was configured as follows: a full MS1 scan was acquired over an m/z range of 380-980 at a resolution of 240K, after which the m/z range was divided into several consecutive isolation windows. All precursor ions within each window were cyclically fragmented to generate MS2 spectra for subsequent label-free quantification. MS2 scans covered an m/z range of 150-2000. Higher-energy collisional dissociation was performed with a normalized collision energy of 25% and an isolation window of 2 m/z.

The MS files were processed using DIA-NN software (1.8.1). Carbamidomethylation was set as a fixed modification, while oxidation (M) and acetylation (protein N-term) were specified as variable modifications. Trypsin was used as the protease, allowing up to two missed cleavages. The false discovery rate was fixed at 0.01 at both the peptide-spectrum match and peptide levels. Peptide identification was performed with an initial precursor mass tolerance of 20 ppm and a fragment mass tolerance of 20 ppm, while all other parameters were kept at their default values.

2.6 Animal experimental design

Female C57BL/6J mice (specific-pathogen-free, 8 weeks, 20-22 g) were purchased from Rise Mice Biotechnology Co., Ltd. (Zhaoqing, China). All mice were housed under specific pathogen-free conditions at 25 ± 2°C with 55-65% humidity and a 12 h light/dark cycle, with free access to food and water. All experimental procedures were approved by the Experimental Animal Ethics Committee of Guangdong Medical University (Approval No. GDMU-2024-000021).

A priori sample size calculation was performed to determine the required number of animals. Based on effect sizes from preliminary experiments and literature reports, with the significance level (α) set at 0.05 and statistical power (1-β) at 0.80, the minimum sample size was estimated to ensure adequate statistical power (Supplementary Table S1). According to this preset sample size per group, animals were selected in the order of generated random numbers and assigned to their respective treatment groups. To simulate the pathological state of disordered bone-lipid metabolism, animal models were established based on previous reports [17, 18]. The mice were divided into a Sham group (n = 5), which was fed a normal diet, and a Model groups (n = 20), which was fed a high-fat diet. All mice in the Model group subsequently underwent bilateral OVX to induce osteoporosis, as previously described [19], while the Sham group received sham surgery. One week after modeling, the Model group was further randomly divided into 4 subgroups (n = 5): Model, CPFM-L (1.16 g/kg), CPFM-H (3.48 g/kg), Estradiol (E2, 50 μg/kg). The dosages of CPFM were calculated based on the human equivalent dose of fish maw [20](9 g/70 kg = 0.128 g/kg), converted to a mouse dose using a factor of 9.1, resulting in a low dose of 1.16 g/kg and a high dose of 3.48 g/kg (3× the low dose). All drug-treated groups received daily oral gavage of CPFM and E2 at their designated doses, while the Sham and Model groups received an equal volume of distilled water, with the volume adjusted according to body weight. All treatments were administered daily by gavage for 12 weeks. At the end of the study, all mice were anesthetized with tribromoethanol (200 mg/kg, i.p.) and euthanized for sample collection.

2.7 Assessment of biochemical and biometric parameters

Body weight was monitored periodically. Final blood samples were analyzed for total cholesterol (T-CHO), triglycerides (TG), and alkaline phosphatase (ALP) with commercial kits (Nanjing Jiancheng Bioengineering Institute, China). After dissection, organs (lungs, livers, kidneys, hearts, spleens) and inguinal fat pads were weighed to determine organ indices (organ weight/body weight × 100%). Bilateral femur, tibia, and fat pad specimens were snap-frozen and stored at -80°C.

2.8 High-resolution microcomputed tomography (μ-CT) analysis

Isolated femora were fixed in 4% buffered formaldehyde at 4°C for 8 h. Bone microarchitecture was assessed using a high-resolution micro-CT system (SkyScan1276, Bruker, Belgium). Scans were performed with the following parameters: voxel size 15.83 μm³, X-ray voltage 40 kV, current 200 μA, and integration time 284 ms. Three-dimensional visualization was conducted using CTVol software (v2.0, SkyScan). For trabecular bone analysis, a region of interest (ROI) encompassing 100 consecutive slices was selected distal to the growth plate, consistent with a previous study [21]. The images were segmented and binarized, and 3D morphometric parameters were calculated in a batch process using CTan software (v1.16, SkyScan). The evaluated parameters for trabecular bone included trabecular bone volume/total volume (Tb.BV/TV), trabecular bone density (Tb.BMD), thickness (Tb.Th), and number (Tb.N). Cortical bone parameters, specifically cortical thickness (Ct.Th) and cortical density (Ct.BMD), were determined using an automatic thresholding algorithm.

2.9 Three-point bending test

Bone mechanical quality test was carried out as previously described [22]. The tensile strength of the femoral cortical bone was tested using a TA ElectroForce 3200 instrument (TA Instruments, New Castle, DE, United States). The following parameters were measured: elastic stress, stiffness, elastic modulus, elastic load, bending strength/elastic modulus (B/E), maximum load. The corresponding stress-strain curve were created with Origin 2024 software.

2.10 Histopathological analysis

Femur and inguinal fat pad samples were dehydrated, cleared, and embedded in paraffin (Leica, Germany). Sections of 4 μm thickness were prepared for subsequent staining procedures. For general histology, sections were stained with Hematoxylin and Eosin (H&E). To assess bone formation, Masson's trichrome staining was performed, with newly formed bone appearing blue. For immunohistochemical analysis, deparaffinized sections were blocked with 5% goat serum (Servicebio, China) and incubated overnight at 4°C with the following primary antibodies: anti- bone gamma-carboxyglutamic acid-containing protein (BGLAP) (1:50) and anti-PPARγ (1:100). After washing, the sections were incubated with a secondary antibody, and antigen binding was visualized using a diaminobenzidine chromogenic kit (Servicebio, China), followed by counterstaining with hematoxylin. All stained sections were examined under a light microscope.

2.11 Cell culture and treatment

BMSCs were obtained from Procell Life Science & Technology Co., Ltd (Wuhan, China, CP-M131). All cells were maintained at 37°C in a humidified 5% CO_2 atmosphere. BMSCs were cultured in BMSCs growth medium (Procell, Wuhan, China). To induce adipogenesis, the cells were treated with BMSCs adipogenic differentiation medium (BMSCs-ADM). The differentiation process was completed after 1 week, with the BMSCs-AMD being changed every 3 days [23]. To induce bone differentiation, the cells were treated with BMSCs osteogenic differentiation medium (BMSCs-ODM). After 14 to 21 days of culture in osteogenic conditions, the ability for osteogenic differentiation was studied [24].

For viability assays, cells were seeded in 96-well plates and treated with various concentrations of CPFM peptides (0, 50, 100, 250, 500, 750, 1000 μg/mL) for 24 h. Cell viability was then assessed using the Cell Counting Kit-8 (CCK-8, Beyotime, Shanghai, China) according to the manufacturer's instructions. A microplate reader was used to measure the optical density (OD 450 nm) values.

2.12 Oil Red O (ORO) staining

Lipid accumulation in differentiated adipocytes was assessed by ORO staining. On day 7 of differentiation, the culture medium was removed, and the cells were gently washed with phosphate-buffered saline (PBS). The cell monolayer was then fixed with 4% paraformaldehyde at room temperature for 15 min. After fixation, the cells were stained with a filtered ORO working solution (Sigma-Aldrich, St. Louis, MO, USA) for 1 h. Subsequently, the staining solution was removed, and the cells were thoroughly rinsed with

distilled water to remove non-specific staining. The stained lipid droplets were visualized and imaged under a light microscope.

2.13 Osteoblast differentiation assessment

Osteogenic differentiation of BMSCs was evaluated by ALP and Alizarin Red S (ARS) staining, which indicate early differentiation and late-stage mineralization, respectively. For ALP staining on day 14, cells were washed with PBS and fixed with 4% paraformaldehyde at room temperature for 15 min. After three PBS washes, the fixed cells were incubated with BCIP/NBT substrate (Beyotime, Shanghai, China) in the dark for 2 h, followed by rinsing with distilled water. For ARS staining on day 21, cells were similarly washed, fixed, and stained with 0.5% ARS solution (Solarbio, Beijing, China) until bright red mineralized nodules were visible. The staining solution was then removed, and cells were rinsed thoroughly with distilled water. Stained cells were imaged under a light microscope (Leica Microsystems, Wetzlar, Germany), and photographs were documented for further analysis.

2.14 Reverse transcription quantitative polymerase chain reaction (RT-qPCR)

According to the manufacturer's instructions, TRIzol reagent (Beyotime, Shanghai, China) was used to extract total RNA from tibias or cells in various groups. RNA was reverse-transcribed into cDNA using 5 × PrimeScript RT Master Mix (Takara, Dalian, China) and RNase-free deionized H_2O. Subsequently, RT-qPCR was conducted on cDNA using SYBR Premix Ex Taq II (2 X) (Takara, Dalian, China). The experiments were standardized using β-Actin as the reference gene, and the target gene was analyzed using the $2^{\Delta\Delta Ct}$ method [25]. Primer details were provided in Table 2.

Table 2. PCR primers used in this study.

Primers	Forward sequence (5' to 3')	Reverse sequence (5' to 3')
β-Actin	TATGCTCTCCCTCACGCCATCC	GTCACGCACGATTTCCCTCTCAG
RUNX2	GACTGTGGTTACCGTCATGGC	ACTTGGTTTTTCATAACAGCGGA
COL1α2	GCTCCTCTTAGGGGCCACT	CCACGTCTCACCATTGGGG
RUNX2	GACTGTGGTTACCGTCATGGC	ACTTGGTTTTTCATAACAGCGGA
BGLAP	CTTGGTGCACACCTAGCAGA	CTCCCTCATGTGTTGTCCCT
FASN	TGGCTGGAAGATGGTGATGA	TGGCTGGAAGATGGTGATGA
PPARγ	GGAAAGACAACGGACAAATCAC	TACGGATCGAAACTGGCAC
FABP4	AACACCGAGATTTCCTT	ACACATTCCACCACCAG

2.15 Western blot (WB)

The tibias or cells were lysed using immunoprecipitation assay lysis buffer supplemented with phenylmethylsulfonyl fluoride (Beyotime, Shanghai, China) on ice for 30 min, with levels determined using bicinchoninic acid protein assay kit (SEVEN, Beijing, China). Proteins from each sample underwent 10% sodium dodecyl sulphate-polyacrylamide gel electrophoresis, were transferred to polyvinylidene fluoride membranes and blocked with 5% non-fat dry milk at room temperature for 1 h. The membranes were incubated with primary antibodies against β-actin (1:5000), RUNX2 (1:2000), BGLAP (1:500), collagen type I alpha 2 (COL1α2) (1:1000), PPARγ (1:1000), FABP4 (1:1000) and fatty acid synthase (FASN)

(1:1000) overnight at 4 °C. Following this, the membranes underwent three washes in Tris-buffered saline-Tween and were incubated with the relevant horseradish peroxidase-conjugated secondary antibodies at room temperature for 2 h. The detection of protein expression was performed with the Tanon 5200 Image Analyzer (Tanon, Shanghai, China) using a chemiluminescent reagent for specific proteins.

2.16 Screening of potential bioactive peptides

The bioactive potential of absorbable peptides was further examined by employing PeptideRanker (http://distilldeep.ucd.ie/PeptideRanker/), with labeling those predicted above a 0.5 threshold as bioactive. Cell penetrating peptides (CPP) (http://distilldeep.ucd.ie/CPPpred/) were currently employed in a wide range of cell-related research and clinical treatment fields [26]. The cell-penetrating probability was predicted by CPPpred, with peptides scoring above 0.33 labeled as high cell-penetrating ability. Using the ADMETlab 3.0 database (https://admetmesh.scbdd.com/), the absorption, distribution, metabolism, excretion, and toxicity (ADMET) properties of the selected peptides were evaluated. LogP (calculated by ChamDraw 20.0) values were used to evaluate the potential biological properties and the hydrophilicity. The toxicity of peptides was assessed using ToxinPred (https://webs.iiitd.edu.in/raghava/toxinpred/).

2.17 Fluorenylmethyloxycarbonyl (Fmoc) solid-phase synthesis method

FLLL peptide was synthesized using an Fmoc solid-phase synthesis method. Firstly, 2-Chlorotrityl Chloride Resin was mixed with dimethylformamide, add Fmoc-Leu-OH and N, N-diisopropylethylamine, followed by deprotection, detection, washing, condensation, and re-detection. Fmoc-Leu-OH and Fmoc-Phe-OH were linked in sequence from C-terminus to N-terminus, rinsed, and then the protecting group was removed. Following cleavage, drying, purification, and lyophilization, the peptide was identified using MS and high-performance liquid chromatography analysis and stored in a sealed container at -20°C.

2.18 Rescue experiment of FLLL against rosiglitazone-induced inhibition of osteogenesis

To investigate whether FLLL could reverse the inhibitory effect of PPARγ activation on RUNX2 expression and osteogenic differentiation, a rescue experiment was performed using an osteogenic differentiation model of BMSCs. Five experimental groups were established: Blank group (basal medium only), Control group (osteogenic induction medium with DMSO as vehicle), FLLL group (osteogenic induction medium + 100 μM FLLL), PPARγ agonist group (osteogenic induction medium + 10 μM rosiglitazone [27]), and Rescue group (osteogenic induction medium + 10 μM rosiglitazone + 100 μM FLLL). All treatments were added simultaneously at the start of induction. On day 14, cells were subjected to ALP staining, and total RNA and protein were extracted for RT-qPCR and western blotting to assess RUNX2 expression. On day 21, ARS staining was performed to evaluate late-stage mineralization.

2.19 Molecular docking

Molecular docking was performed using AutoDock Vina (v1.5.7) to evaluate the binding interactions between the receptor and ligands. The receptor structure was preprocessed by removing water molecules and co-crystallized ligands, followed by energy minimization. Ligand structures were obtained and prepared

with appropriate parameterization. Semi-flexible docking simulations were carried out, and the resulting conformations were saved in PDBQT format. Binding affinity was expressed in kcal/mol, with more negative values indicating stronger interactions. A binding energy threshold of ≤-5.0 kcal/mol was applied to identify high-affinity binders, consistent with established criteria [28]. The top-ranked docking pose was visualized and analyzed using PyMOL.

2.20 Surface Plasmon Resonance (SPR) Analysis

SPR experiments were performed on a Biacore T100 instrument (Cytiva). Series S CM5 or C5 sensor chips (BR100530 and BR100399, respectively) were equilibrated from 4 °C to room temperature for 1 h before use. The system was primed with running buffer (1× PBST) for at least three cycles. For His-tagged ligand immobilization, the NTA capture method was used: ligand (≥40 μg/mL, ≥100 μL) was injected at 10 μL/min for 120 s. For polyclonal antibody immobilization, amine coupling was performed after pH scouting with 10 mM sodium acetate (optimal pH determined by highest response), followed by activation with EDC/NHS and deactivation with ethanolamine. For kinetic analysis, serially diluted peptides (≥1 mg/mL stock, ≥200 μL) were injected at 30 μL/min (association 120 s, dissociation 180 s). The surface was regenerated with 1 mM glycine-HCl (pH 1.5-3.0) for 30 s after each cycle. Data were double-referenced (subtracting reference channel and zero-concentration signals) and fitted globally using BIAevaluation software with a 1:1 Langmuir binding model [29].

2.21 Data analysis

Experimental data were analyzed and graphically processed using GraphPad Prism 8.0 software (GraphPad Prism Software Inc., CA, USA). The data were shown as mean ± standard deviation and analyzed using *one-way ANOVA* with *Tukey's post hoc test*. A statistically significant difference was considered when the p-value＜0.05.

3. Result

3.1 Protein composition and digestion-released peptide profiles of CPFM

The base peak chromatogram (BPC) was presented in Fig. 2A. The majority of CPFM proteins were distributed within the 0-100 kDa range (Fig. 2B). CPFM was subjected to the INFOGEST 2.0 protocol to obtain absorbable peptides for further investigation [15]. The BPC of the resulting peptides were displayed in Fig. 2C. After digestion, the molecular weight distribution shifted markedly towards small-molecular peptides (0.5-1 kDa), representing 84.6% of the total peptides (Fig. 2D). And, CPFM was rich in heptapeptides (20%), octapeptides (18%), tetrapeptides (16%), and nonapeptides (16%) (Fig. 2E). Thus, we aimed to further investigate the functionality of CPFM and screen for potential bioactive peptides.

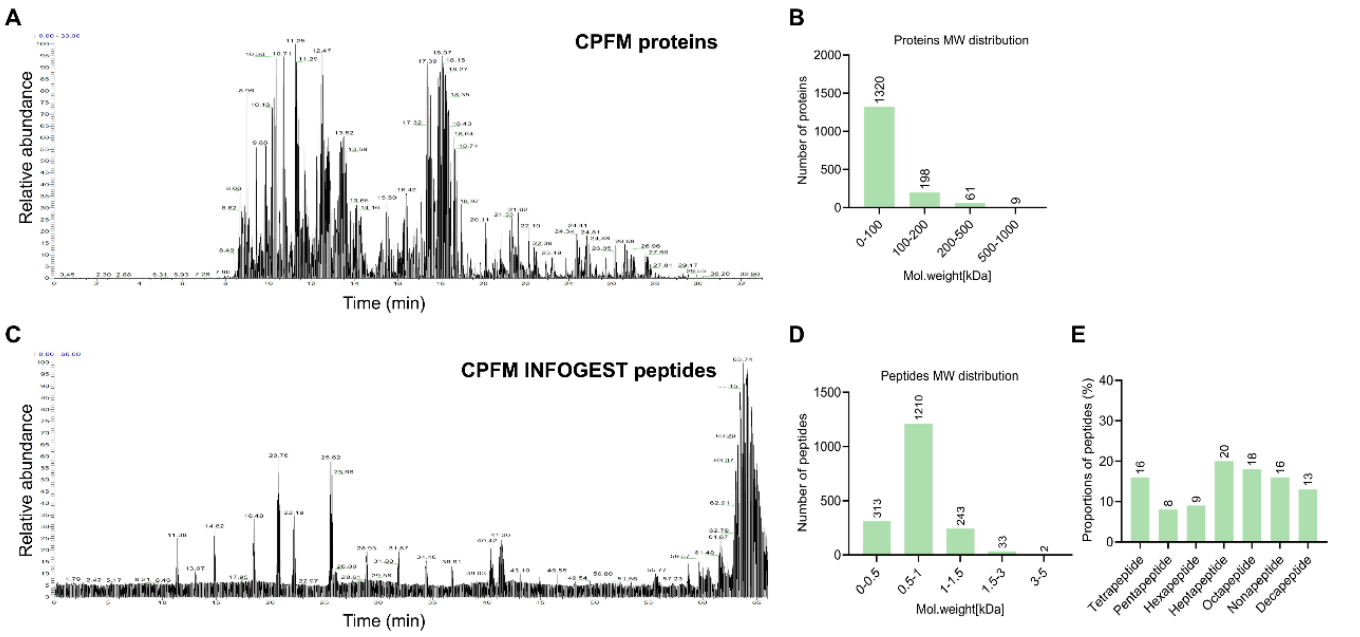

Fig. 2. LC-MS/MS-based chemical profiling of CPFM before and after INFOGEST simulated digestion. Analysis prior to INFOGEST digestion: (A) Base peak chromatograms (BPC) of CPFM proteins, (B) Molecular weight distribution of proteins. Analysis following INFOGEST digestion: (C) BPC of CPFM peptides, (D) Molecular weight distribution of peptides, (E) Proportion of different peptide types.

3.2 CPFM peptides alleviated fat accumulation in OVX osteoporotic mice

We utilized an established mouse model combining OVX with a high-fat diet [19], to assess the impact of CPFM peptides on bone-fat balance in postmenopausal osteoporosis (Fig. 3A). The high-fat diet significantly increased body weight in OVX mice (Fig. 3B). Treatments with CPFM peptides, significantly attenuated this weight gain without affecting overall food intake (Fig. S1A-D).

Consistent with the body weight data, the mass of inguinal fat (representing visceral fat) was significantly increased in OVX mice [30]. H&E staining and subsequent quantification corroborated the anti-obesity effects of CPFM peptides treatments (Fig. 3C). The adipocyte area was significantly reduced in the CPFM groups. Inguinal fat index showed the same results (Fig. 3D and 3E).

At the systemic level, the T-CHO and TG levels were significantly elevated in OVX mice. CPFM peptides normalized these levels, demonstrating an improvement in the overall lipid profile (Fig. 3F and 3G). Critically, none of the treatments induced significant changes in major organ indices, indicating no overt toxicity (Fig. S1E-S1I).

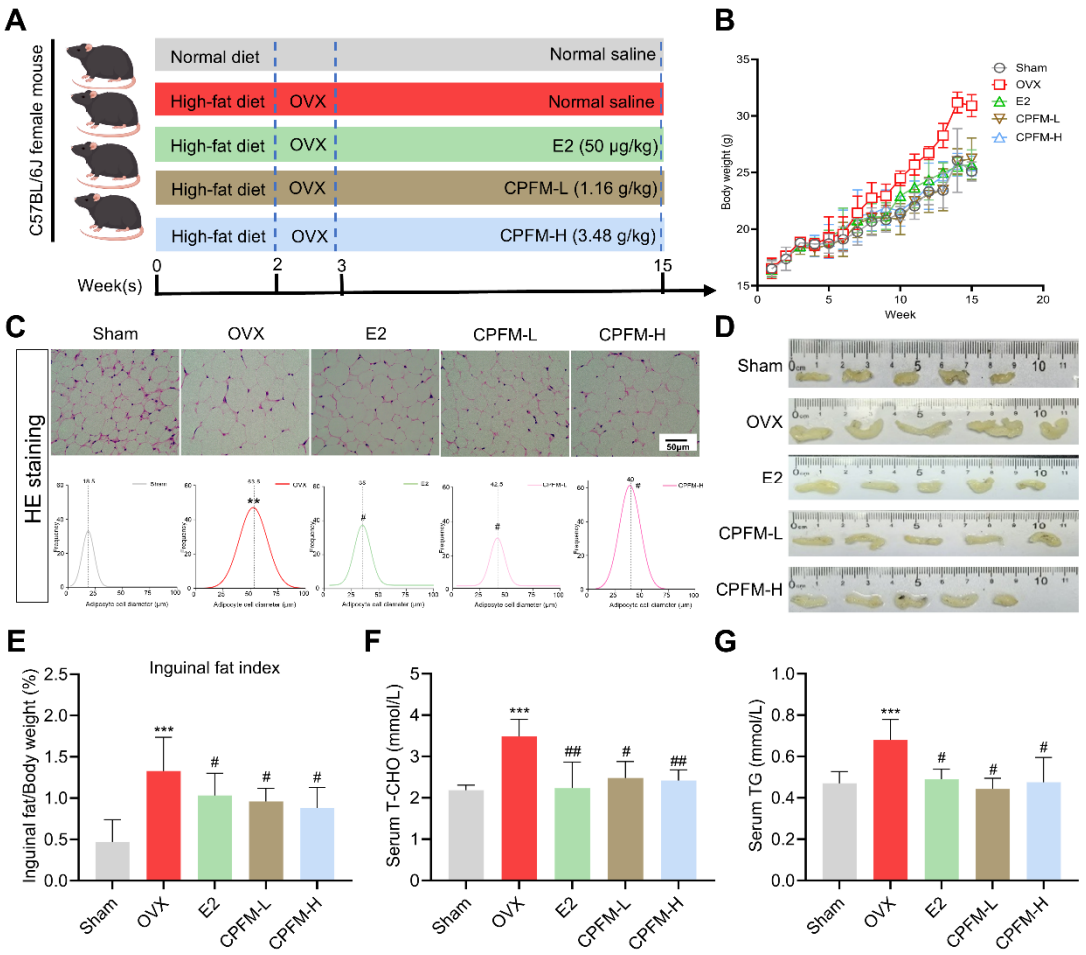

Fig. 3. Effects of CPFM peptides on fat accumulation in ovariectomized osteoporosis mice. The drug treatment group was given the corresponding dose once a day by gavage for 12 weeks. (A) Animal experiment process, (B) Weight changes per week, (C) HE staining and quantitative analysis of inguinal fat, (D-E) Representative gross images of abdominal adipose tissue inguinal fat pads and the inguinal fat index, (F-G) The levels of serum total cholesterol (T-CHO) and triglyceride (TG). The histological sections were observed and photographed at magnification (20×, 50 μm). The results were presented as mean ± SD (n = 5), $^{**}P < 0.01$, $^{***}P < 0.001$ vs. Sham group, $^{\#}P < 0.05$, $^{\#\#}P < 0.01$ vs. OVX group.

3.3 CPFM peptides exerted a protective effect on bone mass loss and bone microstructure in OVX osteoporotic mice

Micro-CT analysis confirmed that OVX induced severe trabecular bone loss in the distal femur. This bone loss was ameliorated by 12-week treatment CPFM peptides (Fig. 4A). Our results indicated that CPFM peptides increased Tb.BMD, Tb.N, and BV/TV (Fig. 4B-D) and enhanced Ct.BMD, Ct.Th, and Tb.Th (Fig. S2A-C). Furthermore, both ALP activity (Fig. 4E) and bone index (Fig. S2D) were significantly elevated in CPFM groups, indicating enhanced bone formation.

Biomechanical testing confirmed that bones treated with CPFM peptides exhibited superior hardness and elasticity compared to the OVX group, as evidenced by overall improvements in bone strength parameters (Fig. 4F-I, S2E-H). H&E and Masson's trichrome staining further revealed that CPFM treatment increased trabecular number and promoted collagen deposition (Fig. 4J-L). In line with this, the results were simultaneously verified *in vitro*.

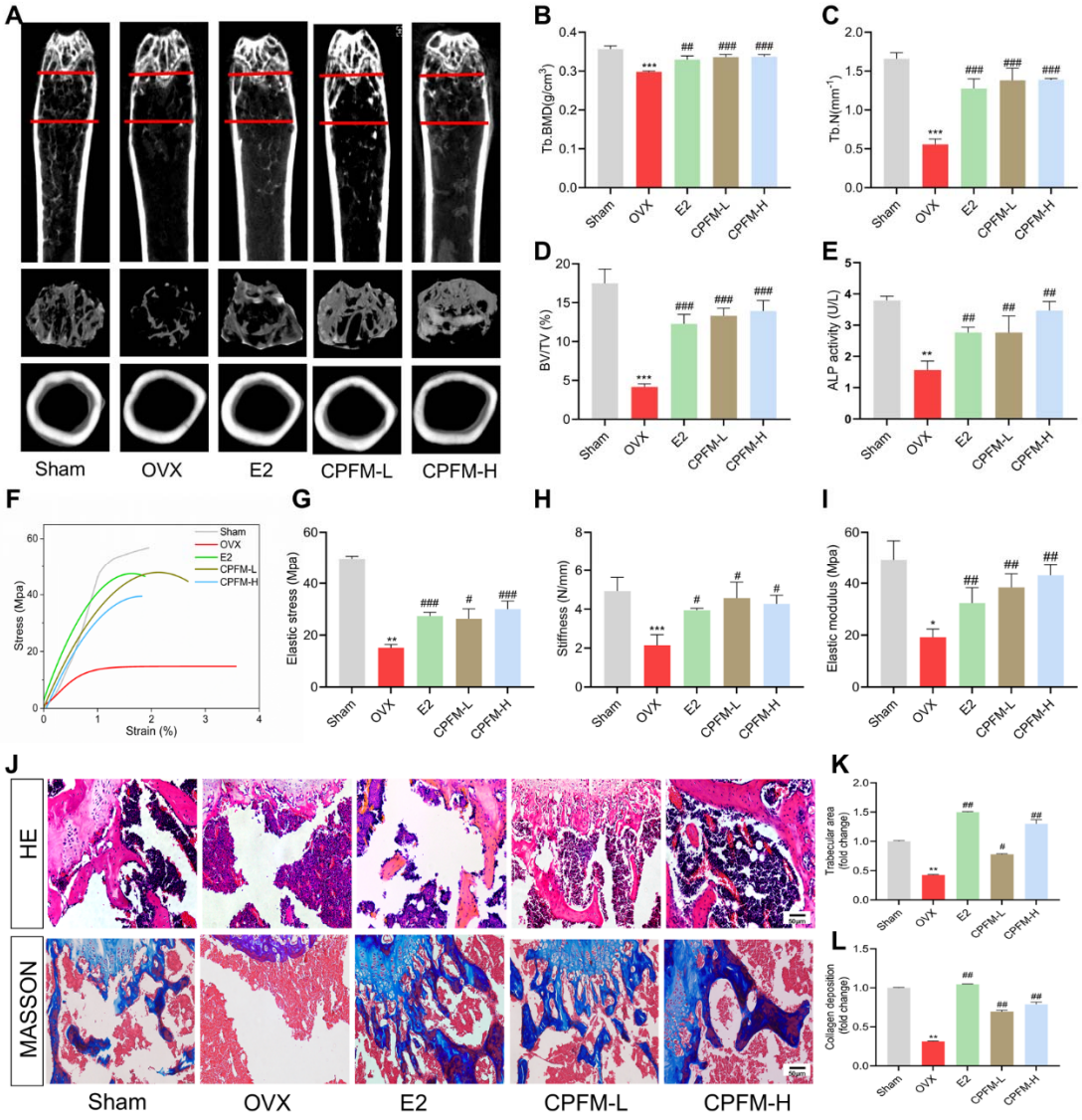

Fig. 4. Effects of CPFM peptides on bone mass loss and bone microstructure in ovariectomized osteoporosis mice. (A) Microstructure of mouse femoral tissue scanned by 3D reconstruction micro-CT, (B-D) Quantitative analysis of trabecular bone microstructure: trabecular bone mineral density (Tb. BMD), trabecular number (Tb. N), and bone volume fraction (BV/TV), (E) Quantitative analysis of alkaline phosphatase (ALP) activity, (F) Stress-strain curve of femur measured by the three-point bending test, (G-I) Mechanical properties determined by three-point bending: elastic stress, stiffness, and elastic modulus, (J-L) Histomorphometric analysis: (J) HE and Masson staining, with quantification of (K) trabecular bone area and (L) collagen deposition. The histological sections were observed and photographed at magnification (20×, 50 μm). The results were presented as mean ± SD (n = 3), $^{*}P < 0.05$, $^{**}P < 0.01$, $^{***}P < 0.001$ vs. Sham group, $^{\#}P < 0.05$, $^{\#\#}P < 0.01$, $^{\#\#\#}P < 0.001$ vs. OVX group.

3.4 CPFM peptides inhibited adipogenesis while promoting osteogenesis in vitro.

CCK-8 assays demonstrated no significant cytotoxicity of CPFM peptides (50-500 μg/mL, 24 h) toward either cell line (Fig. 5A). Pharmacological evaluation at 100, 250, and 500 μg/mL (designated as low, medium, and high doses, respectively) revealed distinct bioactivities. CPFM peptides had no effect on the proliferation of BMSC-derived adipocytes or osteoblasts (Fig. 5B-C) but dose-dependently suppressed adipogenic differentiation (Fig. 5D and 5E). Conversely, ALP activity, an early osteogenic marker, was dose-dependently enhanced by CPFM peptides. ARS staining, indicating late-stage mineralization, was significantly increased by CPFM-M, and CPFM-H (Fig. 5F-5H). Our results indicated that CPFM peptides

selectively promote BMSCs osteogenesis while suppressing BMSCs adipogenesis *in vitro*. Subsequently, we investigated the underlying mechanism of CPFM peptides and screened FLLL as a potential bioactive peptide.

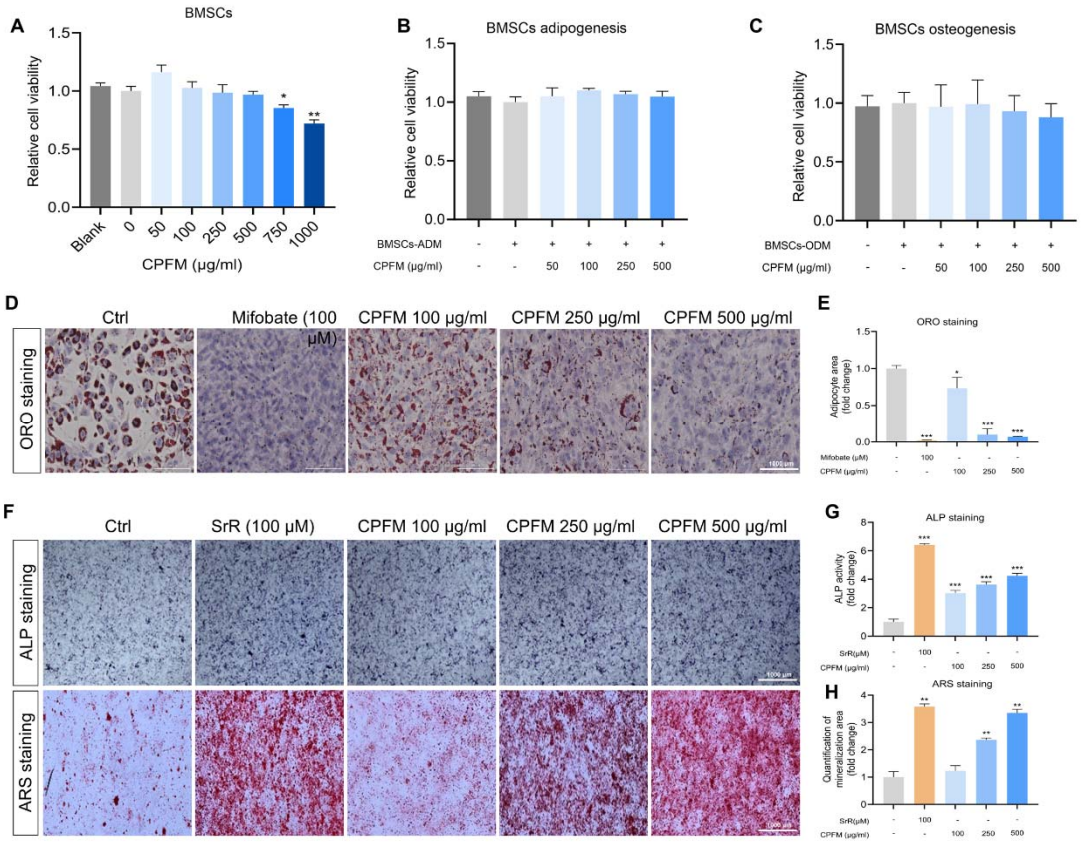

Fig. 5. Effects of CPFM peptides on differentiation of mouse bone marrow mesenchymal stem cells (BMSCs) *in vitro*. CPFM peptide samples were prepared using the INFOGEST *in vitro* simulated digestion method, followed by pharmacodynamic studies. (A-C) The effects of different concentrations of CPFM peptides on BMSCs were determined by CCK-8, respectively, (D-E) Adipogenesis shown by Oil Red O (ORO) staining of lipid droplets and quantified by adipocyte area, (F-H) Osteogenesis shown by early-stage (ALP staining) and late-stage (ARS staining) markers and quantified by adipocyte area. The stained cells were observed and imaged at magnification (4×, 1000 μm or 20×, 100 μm, respectively). The results were presented as mean ± SD ($n = 3$), $^{*}P < 0.05$, $^{**}P < 0.01$, $^{***}P < 0.001$ vs. Blank group or Ctrl group.

3.5 CPFM peptides promoted the osteogenic pathway and inhibited the adipogenic pathway.

In GO enrichment analysis, the differential proteins of biological process (BP), cellular composition (CC), and molecular function (MF) were screened, respectively (Fig. 6A). Among them, BP was mainly involved in localization, lipid metabolic process, cellular lipid metabolic process, *etc*. CC was mainly involved in cytoplasm, intracellular anatomical structure, *etc*. MF was mainly involved in lipid binding, phospholipid binding, enzyme activator activity, *etc*. The differential proteins in KEGG were screened based on the *P*-value (Fig. 6B). The results above suggested a strong correlation between the lipid metabolism disorder and bone diseases. Compared with the Sham group, 22 proteins were downregulated in the Model group, and their expression was restored to normal levels following CPFM treatment. Conversely, 68 proteins were abnormally upregulated in the Model group, and their expression was suppressed after CPFM intervention (Fig. 6C). The osteogenic markers (RUNX2, BGLAP, COL1A2) and adipogenic factors (PPARG, FASN, FABP4) were directly connected to multiple differentially expressed proteins, suggesting their significant regulatory roles in osteogenic and adipogenic pathways, respectively (Fig. 6D-E).

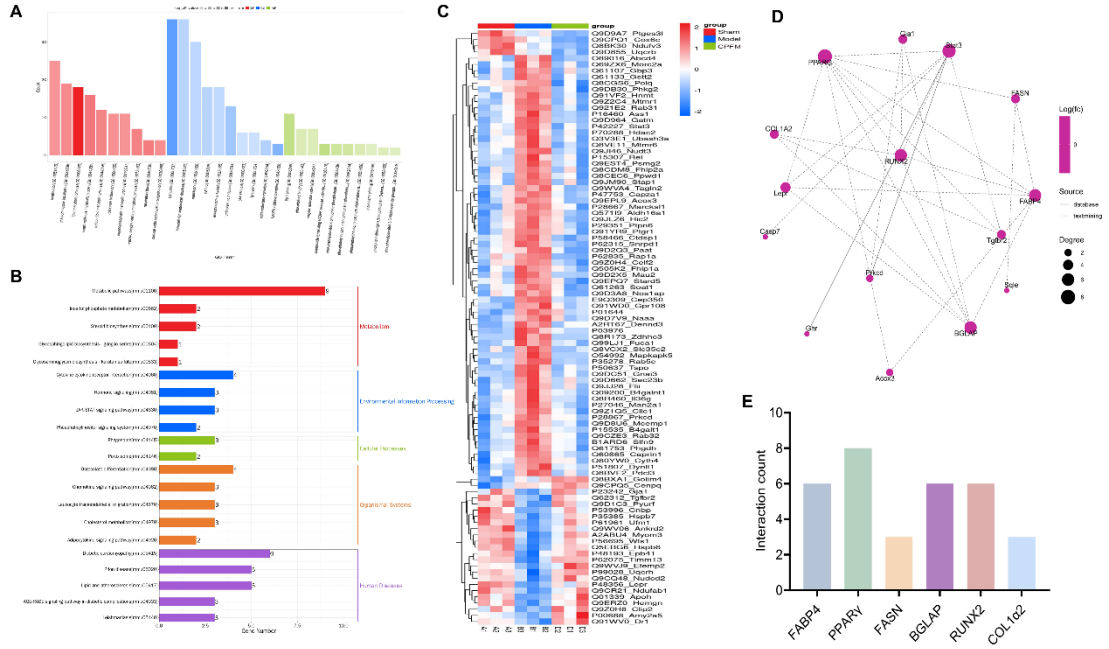

Fig. 6. Differential proteomics and network analysis of tibial tissues following CPFM peptides intervention. (A) GO enrichment analysis of differentially expressed proteins in biological process, cellular component, and molecular function categories, (B) KEGG pathway enrichment analysis of differentially expressed proteins, (C) Venn diagram showing numbers of proteins with differential expression in Sham, Model and CPFM groups, (D-E) Protein interaction networks centered on osteogenic markers (RUNX2, BGLAP, COL1A2) (D) and adipogenic factors (PPARG, FASN, FABP4). Data are from tibiae proteomics (n = 3).

Further experiments were performed to explored the impact of CPFM peptides on bone-fat mechanism. *In vivo*, CPFM peptides downregulated mRNA and protein expression of FASN, PPARγ and FABP4 in tibial tissues (Fig. 7A-E). In contrast, mRNA and protein levels of key osteogenic markers (COL1α2, Runx2 and BGLAP) were elevated by CPFM peptides in tibial tissues (Fig. 7F-J). To this end, we further screened and validated the bioactive peptide FLLL.

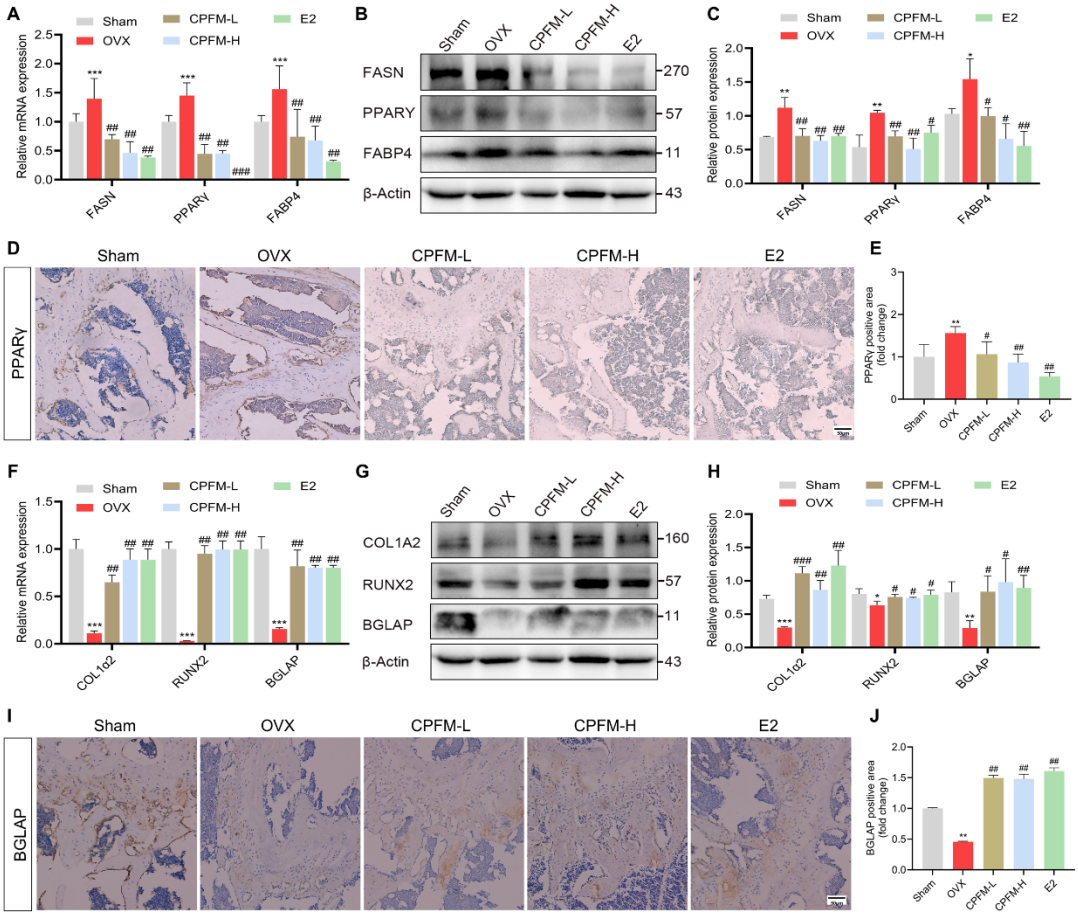

Fig. 7. Effects of CPFM peptides on adipogenesis and osteogenesis in osteoporosis. (A) mRNA levels of adipogenic factors (FASN, PPARγ, FABP4) in tibia tissue, (B-C) Western blot analysis of adipogenic protein levels, (D) Representative immunohistochemical (IHC) staining images for PPARγ, (E) Quantitative analysis of PPARγ-positive area; (F) mRNA levels of osteogenic markers (COL1α2, Runx2, BGLAP) in tibia tissue. (G-H) Western blot analysis of osteogenic protein levels, (I) Representative IHC staining images for BGLAP, (J) Quantitative analysis of BGLAP-positive area. The stained cells were observed and imaged at magnification (20×, 50 μm). The results were presented as mean ± SD ($n = 3$), $^{*}P < 0.05$, $^{**}P < 0.01$, $^{***}P < 0.001$ vs. Sham group, $^{\#}P < 0.05$, $^{\#\#}P < 0.01$, $^{\#\#\#}P < 0.001$ vs. OVX group.

3.6 FLLL was identified as the absorbable bioactive peptide in CPFM

A total of 96 peptides were common to both the serum samples and the INFOGEST digests. (Fig. 8A-C). These common peptides were predominantly low-molecular-weight species, with 99% under 1,000 Da (Fig. 8D). Tetrapeptides accounted for the largest proportion (44%), followed by heptapeptides and pentapeptides (19% each) (Fig. 8E). Among these, the peptide FLLL showed the highest relative abundance (37.8%), rendering it a candidate with considerable research significance (Fig. 8F).

Additionally, ten candidate peptides from Table 3 were systematically evaluated. Four peptides: FLLL, FRKPG, AALGVPPVLL, and PVLLGPPK were exhibited good bioactivity (PeptideRanker > 0.5), high cell permeability (CPPpred > 0.33), good intestinal absorption (HIA+), non-toxicity, no CYP2D6 inhibition risk, and strong membrane permeability. Among these, FLLL was detected in the tibia of OVX-OP mice after oral ingestion of CPFM (Fig. 8G). FLLL, detected in tibiae and possessing favorable drug-like properties, was synthesized and validated by HPLC/MS for functional studies (Fig. 8H and 8I).

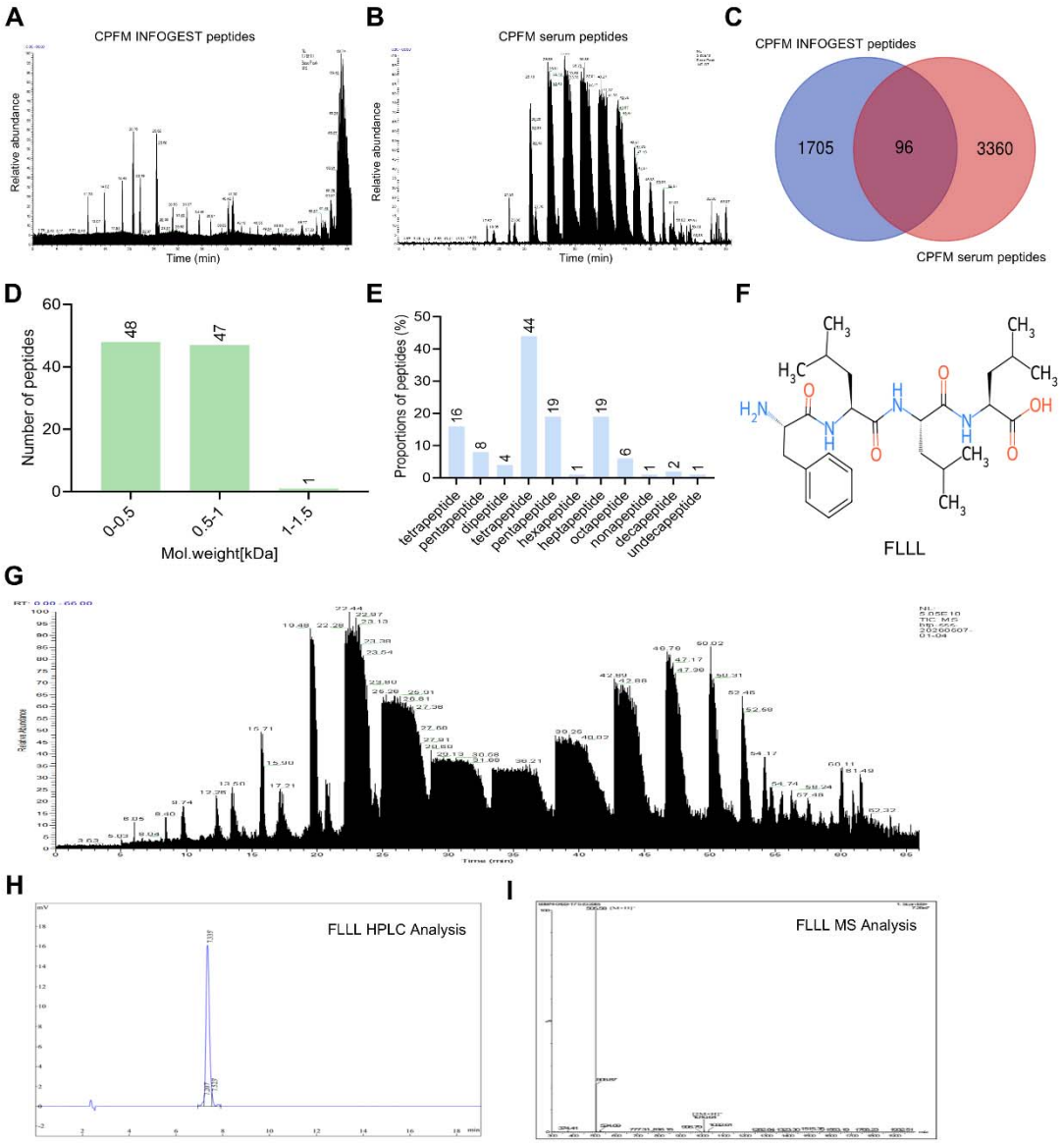

Fig. 8. Identification of absorbable peptide components in CPFM peptides and screening for potential bioactive peptides. (A-B) Base peak chromatograms (BPC) of CPFM after INFOGEST digestion and absorption into the bloodstream, (C) Venn diagram showing the number of peptides and the overlap between the two samples, (D) Molecular weight distribution of the overlapping peptides, (E) Proportional abundance of different peptide sequences of the overlapping peptides, (F) Chemical structure of the most abundant bioactive peptide FLLL, (G) TIC of CPFM-treated mouse tibia, (H-I) Synthetic FLLL was identified by high performance liquid chromatography (HPLC) and mass spectrometry (MS).

Table 3 Screening of the Potential Bioactive Peptides.

Peptide	Relative expression	PeptideRan-ker scores	CPPpred response	HIA	BBB	AOT	CYP2D6 inhibitor	LogP values*	TP
FLLL	37.80%	0.893052	0.410042	+	-	-2.95	Non	2.51	NA
FRKPG	1.70%	0.774710	0.380581	+	-	-3.38	Non	-1.52	NA
AALGVPP VLL	2.20%	0.599333	0.445723	+	-	-3.3	Non	1.98	NA
PVLLGPPK	1.90%	0.539136	0.459005	+	-	-3.18	Non	0.338	NA
QPAG	0.53%	0.520587	0.143862	-	-	-3.55	Non	-4.29	NA
PRKFVLV AGGK	0.74%	0.389686	0.576052	+	-	-2.62	Non	0.191	NA
LLAGPK	1.30%	0.349078	0.547679	+	-	-3.56	Non	0.583	NA
VLVPAPP K	3.50%	0.331505	0.452732	+	-	-3.45	Non	0.662	NA
LPLAAGV	1.30%	0.314207	0.480248	+	-	-3.24	Non	2.378	NA

VL									
PPNK	0.50%	0.448211	0.305531	-	-	-3.72	Non	-3.84	NA

Note: *LogP values: partition coefficient in octanol/water; AOT: Acute toxicity; BBB: Blodd-brain barrier; HIA: Human intestinal absorption; TP: Toxin predict.

3.7 FLLL peptide regulates bone formation and inhibits adipogenesis in BMSCs

FLLL were non-cytotoxic and did not affect the proliferation of BMSC-derived adipocytes and osteoblasts (Fig. 9A-C). Our results demonstrated that both 50 μM (FLLL-L) and 100 μM (FLLL-H) treatments significantly inhibited intracellular lipid accumulation in BMSCs adipocytes (Fig. 9D and 9E). Concurrently, FLLL enhanced osteogenic differentiation in BMSCs, evidenced by increased ALP activity and enhanced mineralized nodule formation as shown by ARS staining (Fig. 9D, 9F and 9G).

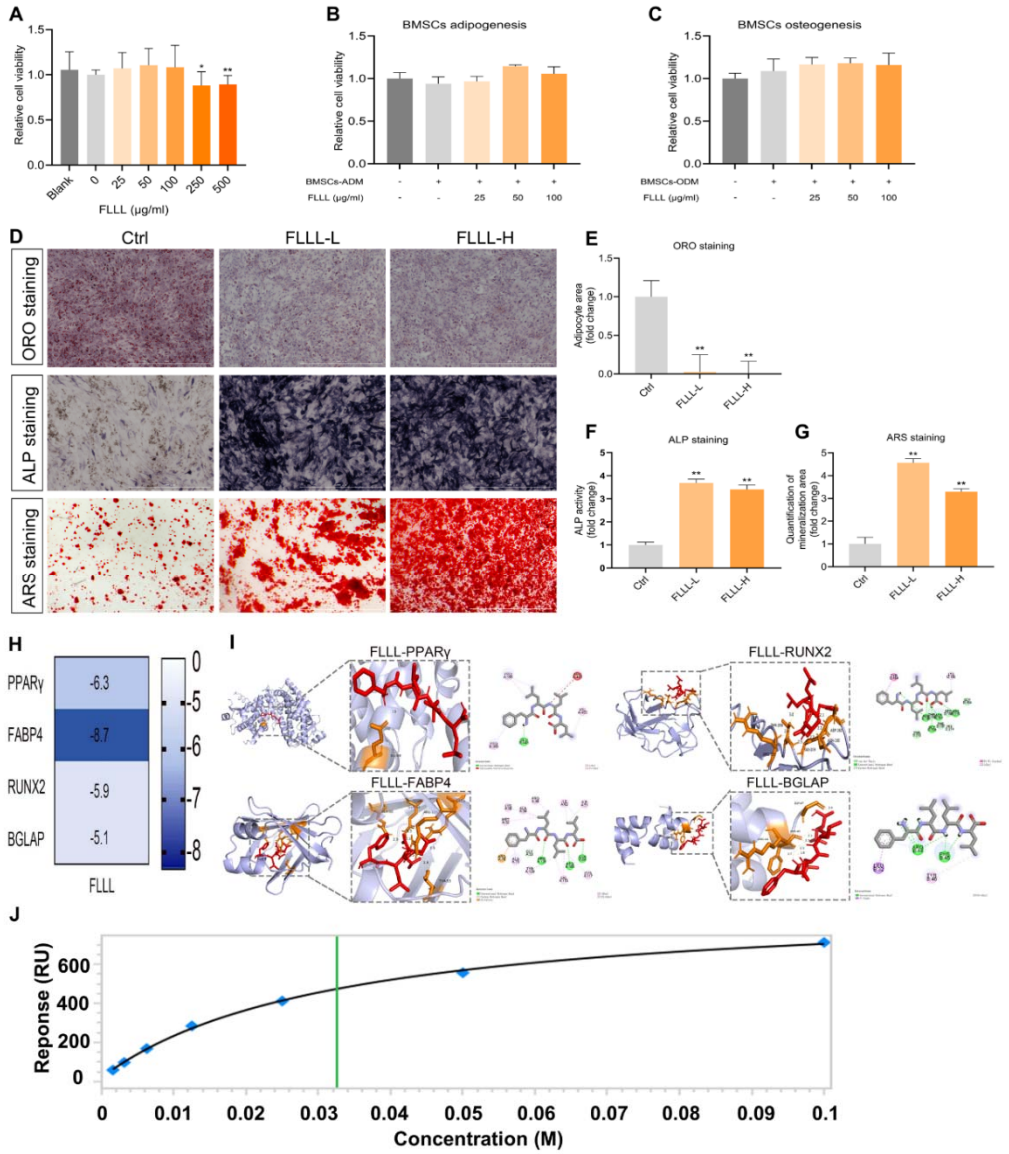

Fig. 9. Effects of FLLL peptide on BMSCs *in vitro*. (A-C) The effects of different concentrations of FLLL peptide on BMSCs were determined by CCK-8, respectively, (D) Representative images of cytochemical staining: oil red O (ORO) for adipocytes, alkaline phosphatase (ALP) and alizarin red S (ARS) for osteoblasts, (E) Quantification of adipocyte area from ORO staining, (F) Quantification of ALP activity, (G) Quantification of mineralized nodule area from ARS staining, (H) Docking scores of the FLLL peptide against adipogenic (PPARγ, FABP4) and osteogenic (Runx2, BGLAP) transcription factors. (I) Representative three-dimensional visualization of the binding poses between FLLL and the targets, (J) Steady-state affinity analysis of FLLL binding to RUNX2 using a 1:1 Langmuir model yielded a KD of 32.52 μM. The stained cells were observed and imaged at magnification (4×, 1000 μm). The results were presented as mean ± SD ($n = 3$), *$P < 0.05$, **$P < 0.01$ vs. Blank group or Ctrl group.

Docking suggested potential binding modes that may contribute to the observed phenotypes. Stable complexes were observed between FLLL and key regulators of adipogenesis and osteogenesis, with calculated binding energies of -6.3 kcal/mol with PPARγ, -8.7 kcal/mol with FABP4, -5.9 kcal/mol with RUNX2, and -5.1 kcal/mol with BGLAP (Fig. 9H). Structural analysis suggested specific interaction patterns: hydrogen bonding with Glu448 of PPARγ; three hydrogen bonds with Arg126, Arg106, and Gln95 of FABP4; six hydrogen bonds with Asn160, Gly159, and Asp161 of RUNX2; and six hydrogen bonds with Arg44 and Phe45 of BGLAP (Fig. 9I). Additional hydrophobic interactions and π-cation/π-sigma contacts further stabilized these complexes, providing a structural basis for dual regulatory function of FLLL through complementary non-covalent forces. Nevertheless, further biophysical and functional validation is required.

We performed surface plasmon resonance experiments to evaluate the direct binding between FLLL and RUNX2. The binding affinity (KD), which reflects the strength of the interaction between ligand and analyte. The results showed that FLLL bound directly to RUNX2, with KD values in the micromolar range: 32.52 μM for RUNX2 (Fig. 9J). Therefore, we speculate that FLLL directly interacts with RUNX2 and enhances its activity, which may facilitate osteogenic differentiation and potentially alleviate osteoporosis.

3.8 FLLL peptide regulated bone-fat balance via PPARγ/RUNX2 axis

In vivo, FLLL downregulated mRNA and protein expression of FASN, PPARγ and FABP4, and in BMSCs (Fig. 10A-E). In contrast, mRNA and protein levels of key osteogenic markers (COL1α2, Runx2 and BGLAP) were elevated by FLLL in BMSCs (Fig. 10F-J).

To further investigate the bidirectional effect of FLLL on the bone-fat balance pathway, ALP and ARS staining was performed. As shown in Fig. 10K-M, the Control group showed strong ALP and ARS staining compared to the Blank group, confirming successful osteogenic induction. FLLL group further enhanced the staining, indicating that FLLL promoted both early and late osteogenic differentiation. In contrast, the PPARγ agonist group reduced staining, suggesting inhibition of osteogenic differentiation and mineralization. In the Rescue group, staining was clearly restored, indicating that FLLL reversed the agonist-induced suppression.

We also examined RUNX2 expression by qPCR and Western blot. As shown in Fig. 10N-P, the Control group had significantly higher RUNX2 mRNA and protein levels than the Blank group, confirming successful induction. FLLL group further increased RUNX2 expression. The PPARγ agonist group significantly reduced RUNX2 levels, while the Rescue group showed a clear recovery of RUNX2 expression. This suggests that FLLL can reverse the inhibitory effect of PPARγ activation on RUNX2 expression.

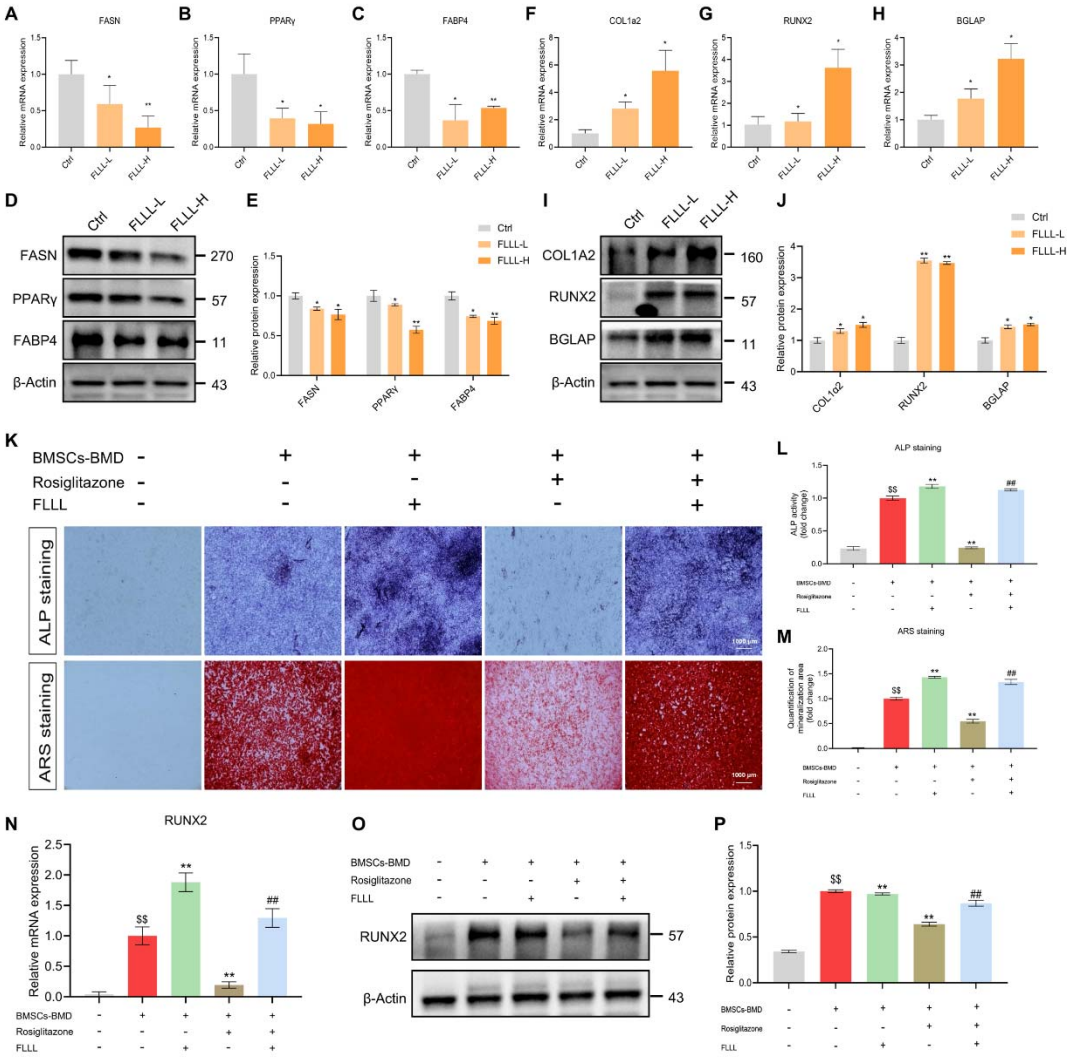

Fig. 10. Effects of FLLL peptide on adipogenic and osteogenic differentiation of BMSCs. BMSCs were induced under adipogenic or osteogenic conditions and treated with FLLL (low or high concentration) or the PPARγ agonist rosiglitazone, either alone or in combination (rescue group). (A-C) Relative mRNA expression levels of adipogenic markers FASN, PPARγ, and FABP4. (D-E) Western blot analysis and semi-quantification of FASN, PPARγ, and FABP4 protein expression. (F-H) Relative mRNA expression levels of osteogenic markers COL1α2, RUNX2, and BGLAP. (I-J) Western blot analysis and semi-quantification of COL1α2, RUNX2, and BGLAP protein expression. (K) Representative images of ALP staining and ARS staining. (L) Semi-quantitative analysis of ALP-positive area. (M) Semi-quantitative analysis of mineralized nodule area from ARS staining. (N) Relative mRNA expression of RUNX2 in the PPARγ agonist rescue experiment. (O-P) Western blot analysis and semi-quantification of RUNX2 protein expression in the rescue experiment. The stained cells were observed and imaged at magnification (4×, 1000 μm). The results were presented as mean ± SD ($n = 3$), $^{*}P < 0.05$, $^{**}P < 0.01$ vs. Ctrl group, $^{*}P < 0.05$, $^{\$\$}P < 0.01$ vs. Blank group, $^{\#\#}P < 0.01$ vs. PPARγ agonist group.

4. Discussion

Postmenopausal osteoporosis (PMOP) is frequently accompanied by abnormal lipid accumulation both systemically and within the bone marrow microenvironment, creating a vicious cycle that exacerbates bone loss [1, 31]. Consequently, targeting the bone-fat metabolic balance has emerged as an important therapeutic strategy. However, existing drugs have certain limitations, driving increasing attention to natural products [19]. Fish-derived peptides are considered promising due to their potential dual regulatory benefits [32]. Fish maw (FM) is rich in collagen peptides, which help promote bone formation, making it an ideal natural health supplement [33]. In traditional practice, heat treatment with clam shell powder (CP) is used to reduce the greasy texture of FM, thereby enhancing its medicinal properties [34]. During this process, FM peptides

undergo the Maillard reaction, forming stable complexes that improve their bioavailability [12]. These findings suggested that CPFM peptides might inhibit lipid metabolism disorders and improve bone formation, yet direct experimental evidence has been lacking. In this study, we provide this evidence by evaluating the anti-osteoporotic efficacy of CPFM peptides using combined *in vivo* and *in vitro* models, and further identify the absorbable tetrapeptide FLLL as a potential active component.

We first characterized the peptide composition of CPFM after INFOGEST simulated digestion, a standardized protocol that mimics human gastrointestinal conditions [15]. Approximately 85% of the peptides had a molecular weight below 1 kDa, indicating high absorption potential [35]. Using an ovariectomized (OVX) mouse model fed a high-fat diet [36], we found that CPFM peptides effectively suppressed weight gain, fat accumulation, adipocyte hypertrophy, and dyslipidemia, consistent with previous reports on collagen-derived peptides [19, 37]. Importantly, CPFM peptides also mitigated bone loss by improving bone microstructure, increasing trabecular number and distribution, and enhancing biomechanical properties.

To investigate the underlying mechanisms, we conducted experiments using bone marrow stromal cells (BMSCs). CPFM peptides inhibited adipogenic differentiation and promoted osteogenic differentiation without affecting cell proliferation. Proteomic analysis revealed that CPFM downregulated adipogenic factors (PPARγ, FABP4, FASN) and upregulated osteogenic markers (RUNX2, COL1α2, BGLAP). Previous studies have established that estrogen deficiency upregulates PPARγ activity, which activates downstream targets such as FABP4 and FASN to promote lipid deposition while suppressing RUNX2-mediated osteogenesis [4, 5]. Our findings, confirmed by RT-qPCR, western blot, and immunohistochemistry, suggest that CPFM counteracts this pathogenic axis.

To identify the active components responsible for these effects, we screened CPFM digests and serum samples. Among the peptides common to both, FLLL showed the highest relative abundance (37.8%) and was prioritized based on its predicted bioactivity, cell-penetrating ability, and favorable ADMET properties. *In vitro*, FLLL fully recapitulated the dual effects of CPFM, promoting osteoblast differentiation and mineralization while inhibiting adipocyte differentiation and lipid droplet accumulation. Molecular docking predicted stable interactions with PPARγ and RUNX2, and surface plasmon resonance confirmed direct binding of FLLL to RUNX2 (KD = 32.5 μM). Given that RUNX2 is negatively regulated by PPARγ [38-40] , we conducted rescue experiments using the PPARγ agonist rosiglitazone. These experiments demonstrated that FLLL reversed the agonist-induced suppression of osteogenic differentiation and mineralization and restored RUNX2 expression at both mRNA and protein levels. These findings indicate that FLLL promotes osteogenic differentiation by binding to RUNX2 and counteracting PPARγ-mediated inhibition in BMSCs.

This study extends prior work on the physicochemical properties of CPFM by demonstrating its *in vivo* and *in vitro* efficacy, elucidating its mechanism on the bone-fat axis, and identifying the absorbable peptide FLLL, thereby underscoring the translational significance of this traditional processing method [12]. However, several limitations should be noted. First, *in vivo* validation of FLLL is still lacking, as all functional data for this peptide are derived from BMSCs culture studies. Second, and future studies should

employ RUNX2 reporter assays or knockout models to explore the regulatory mechanism. Third, the current study has not experimentally validated the direct binding of FLLL to PPARγ, and the evidence for its involvement in the PPARγ pathway remains limited to indirect or network-level observations. Dedicated *in vitro* binding assays and functional studies on PPARγ are therefore warranted to clarify this aspect. Consequently, the precise mechanisms by which CPFM modulates the bone fat balance remain to be fully clarified and merit continued investigation.

5. Conclusion

This study demonstrated that CPFM peptides regulated bone-fat balance in OVX-OP mouse model, reducing bone marrow fat accumulation and improving bone microstructure. Both the CPFM peptides and the tetrapeptide FLLL (identified from CPFM digests) promoted osteogenesis and suppressed adipogenesis in cultured BMSCs. These findings provide a pharmacological basis for further developing CPFM as a functional food for the prevention and treatment of postmenopausal osteoporosis.

Declaration of competing interest

The authors declare that they have no known competing financial interests or personal relationships that could have appeared to influence the work reported in this paper.

Acknowledgments

Economic Development of Marine Economy of Guangdong Province, China (GDNRC[2022]38). The authors thank Hongqiang Li from the Department of Orthopedics, the Affiliated Hospital of Guangdong Medical University, for his valuable assistance.

Reference

[1] H. Niu, M. Zhou, X. Xu, et al., Bone marrow adipose tissue as a critical regulator of postmenopausal osteoporosis-a concise review, Clinical Interventions in Aging. (2024) 1259-1272. https://doi.org/10.2147/CIA.S466446.

[2] A. Elmugadam, G.A. Elfadil, A.I. Hamad, et al., Atherogenic index of plasma and anthropometric measurements among osteoporotic postmenopausal Sudanese women: possible risk for cardiovascular disease, Journal of Aging Research. 2022 (2022) 1545127. https://doi.org/10.1155/2022/1545127.

[3] N.S. Dole, A. Betancourt-Torres, S. Kaya, et al., High-fat and high-carbohydrate diets increase bone fragility through TGF-β-dependent control of osteocyte function, JCI Insight. 9 (2024) e175103. https://doi.org/10.1172/jci.insight.175103.

[4] L. Wang, S. Li, Y. Liu, et al., Greater bone marrow fat and myosteatosis are associated with lower vBMD but not asymptomatic vertebral fracture, Eur Radiol. 33 (2023) 578-586. https://doi.org/10.1007/s00330-022-08979-x.

[5] J.J. Cao, Effects of obesity on bone metabolism, Journal of Orthopaedic Surgery and Research. 6 (2011) 30. https://doi.org/10.1186/1749-799x-6-30.

[6] K. Katzer, J.L. Hill, K.B. McIver, et al., Lipedema and the potential role of estrogen in excessive adipose tissue accumulation, International journal of molecular sciences. 22 (2021) 11720. https://doi.org/10.3390/ijms222111720.

[7] J.E. Rossouw, G.L. Anderson, R.L. Prentice, et al., Risks and benefits of estrogen plus progestin in healthy postmenopausal women: principal results From the Women's Health Initiative randomized controlled trial, Jama. 288 (2002) 321-333. https://doi.org/10.1001/jama.288.3.321.

[8] B. Moosmann, C. Behl, Selenoprotein synthesis and side-effects of statins, The Lancet. 363 (2004) 892-894. https://doi.org/10.1016/s0140-6736(04)15739-5.

[9] I.T. Suryaningtyas, J.-Y. Je, Bioactive peptides from food proteins as potential anti-obesity agents: Mechanisms of action and future perspectives, Trends in Food Science & Technology. 138 (2023) 141-152. https://doi.org/10.1016/j.tifs.2023.06.015.

[10] I.U. Okagu, E.C. Aham, T.P.C. Ezeorba, et al., Osteo-modulatory dietary proteins and peptides: A concise review, Journal of Food Biochemistry. 46 (2022) https://doi.org/10.1111/jfbc.14365.

[11] A. Hou, J. Lv, S. Zhang, et al., Salt processing: a unique and classic technology for Chinese medicine processing, Frontiers in pharmacology. 14 (2023) 1116047. https://doi.org/10.3389/fphar.2023.1116047.

[12] H. Yu, Y. Li, Y. Zhu, et al., Integrative omics analysis: Effects of stir-frying with clamshell powder on the physicochemical properties of fish maw, Food Chem. 491 (2025) https://doi.org/10.1016/j.foodchem.2025.145196.

[13] M. Saravanan, S. Krishnamoorthi, M. Saravanakumar, et al., Investigating Clamshell-Derived NHAp Composites with PLGA and Chitosan for Advancements in Bone Healing, National Conference on Advancement in Materials Processing Technology. (2023) 275-285. https://doi.org/10.1007/978-981-96-7380-3_26.

[14] H.E. Irianto, G. Gyatmi. Fish collagen peptides preparation, characteristics and potential applications. Oxford: Taylor & Francis Group; 2025.

[15] A. Brodkorb, L. Egger, M. Alminger, et al., INFOGEST static *in vitro* simulation of gastrointestinal food digestion, Nature Protocols. 14 (2019) 991-1014. https://doi.org/10.1038/s41596-018-0119-1.

[16] X. Wang, L. Li, G. Zhang, A proteomic study on the protective effect of kaempferol pretreatment against deoxynivalenol-induced intestinal barrier dysfunction in a Caco-2 cell model, Food Funct. 11 (2020) 7266-7279. https://doi.org/10.1039/d0fo01579b.

[17] M. Das, L.G. Ellies, D. Kumar, et al., Time-restricted feeding normalizes hyperinsulinemia to inhibit breast cancer in obese postmenopausal mouse models, Nature Communications. 12 (2021) https://doi.org/10.1038/s41467-020-20743-7.

[18] K. Arisawa, M. Kaneko, A. Matsuoka, et al., Piceatannol prevents obesity and fat accumulation caused by estrogen deficiency in female mice by promoting lipolysis, Nutrients. 15 (2023) 1374.

[19] K. Wu, Z. Gong, L. Zou, et al., *Sargassum integerrimum* inhibits oestrogen deficiency and hyperlipidaemia-induced bone loss by upregulating nuclear factor (erythroid-derived 2)-like 2 in female rats, Journal of Orthopaedic Translation. 19 (2019) 106-117. https://doi.org/10.1016/j.jot.2019.03.002.

[20] L. Deng, R. Liu. Processing of Chinese Materia Medica. Beijing: China Press of Traditional Chinese Medicine; 1993.

[21] Z. Lin, H. He, M. Wang, et al., *MicroRNA-130a* controls bone marrow mesenchymal stem cell differentiation towards the osteoblastic and adipogenic fate, Cell Proliferation. 52 (2019) e12688. https://doi.org/10.1111/cpr.12688.

[22] B. Jyotirmaya, I. Jessica, V. Michael J, et al., Probiotics stimulate bone formation in obese mice via histone methylations, Theranostics. 11 (2021) 8605-8616. https://doi.org/10.7150/thno.63749.

[23] J. Tan, Y. Wang, S. Wang, et al., Label-free quantitative proteomics identifies transforming growth factor β1 (TGF-β1) as an inhibitor of adipogenic transformation in OP9-DL1 cells and primary thymic stromal cells, Cell & Bioscience. 9 (2019) 48. https://doi.org/10.1186/s13578-019-0311-1.

[24] I.R. Orriss, M.O.R. Hajjawi, C. Huesa, et al., Optimisation of the differing conditions required for bone formation *in vitro* by primary osteoblasts from mice and rats, International Journal of Molecular Medicine. 34 (2014) 1201-1208. https://doi.org/10.3892/ijmm.2014.1926.

[25] S. Cao, Y. Wang, Y. Zhang, et al., Naringenin can inhibit the pyroptosis of osteoblasts by activating the Nrf2/HO-1 signaling pathway and alleviate the differentiation disorder of osteoblasts caused by microgravity, J Agr Food Chem. 72 (2024) 25586-25600. https://doi.org/10.1021/acs.jafc.4c05370.

[26] S. Jafari, E. Ahmadian, J.K. Fard, et al., Biomacromolecule based nanoscaffolds for cell therapy, Journal of Drug Delivery Science and Technology. 37 (2017) 61-66. https://doi.org/10.1016/j.jddst.2016.11.006.

[27] G. Viccica, C. Francucci, C. Marcocci, The role of PPARγ for the osteoblastic differentiation, Journal of endocrinological investigation. 33 (2010) 9-12. PMID: 20938219.

[28] Y. Zhang, Z. Zhang, S. Wang, et al., Molecular targets and mechanisms involved in the action of Banxia Shumi decoction in insomnia treatment, Medicine (Baltimore). 102 (2023) e33229. https://doi.org/10.1097/md.0000000000033229.

[29] Z. Wang, M. Wang, M. Zhang, et al., High-affinity SOAT1 ligands remodeled cholesterol metabolism program to inhibit tumor growth, BMC Medicine. 20 (2022) https://doi.org/10.1186/s12916-022-02436-8.

[30] M. Sela, G. Tirza, O. Ravid, et al., NOX1-induced accumulation of reactive oxygen species in abdominal fat-derived mesenchymal stromal cells impinges on long-term proliferation, Cell Death & Disease. 6 (2015) e1728. https://doi.org/10.1038/cddis.2015.84.

[31] J. Li, X. Chen, L. Lu, et al., The relationship between bone marrow adipose tissue and bone metabolism in postmenopausal osteoporosis, Cytokine & growth factor reviews. 52 (2020) 88-98. https://doi.org/10.1016/j.cytogfr.2020.02.003.

[32] A. Alemán, O. Martinez-Alvarez, Marine collagen as a source of bioactive molecules: A review, The Natural Products Journal. 3 (2013) 105-114. https://doi.org/10.2174/2210315511303020005.

[33] C. Mo, Q. Wang, G. Li, et al., Extraction and characterization of pepsin- and acid-soluble collagen from the swim bladders of *Megalonibea fusca*, Mar Drugs. 21 (2023) 159. https://doi.org/10.3390/md21030159.

[34] H. Cai, M. Wang, H. Zhu, et al., Phytochemical component profiling and anti-renal fibrosis effects of crude and salt-stir fried *eucommiae cortex* extracts on renal fibrosis rats caused by high-purine diet, Food Chem. 464 (2025) 141784. https://doi.org/10.1016/j.foodchem.2024.141784.

[35] H. Chen, J. Sun, H. Fang, et al., Food-derived bioactive peptides: health benefits, structure-activity relationships, and translational prospects, Journal of Zhejiang University-SCIENCE B. (2025) 1-22. https://doi.org/10.1631/jzus.B2400106.

[36] F.d.J. Ruiz-López, B.A. Espinosa-Rodríguez, D.A. Silva-Mares, et al., In silico identification of peptides with PPARγ antagonism in protein hydrolysate from rice (Oryza sativa), Pharmaceuticals. 16 (2023) 440. https://doi.org/10.3390/ph16030440.

[37] L. Zhu, W.C. Brown, Q. Cai, et al., Estrogen treatment after ovariectomy protects against fatty liver and may improve pathway-selective insulin resistance, Diabetes. 62 (2013) 424-434. https://doi.org/10.2337/db11-1718.

[38] K. Nomura, Y. Kimira, Y. Osawa, et al., Collagen-derived dipeptide prolyl hydroxyproline directly binds to Foxg1 to change its conformation and inhibit the interaction with Runx2, Bioscience, Biotechnology, and Biochemistry. 83 (2019) 2027-2033. https://doi.org/10.1080/09168451.2019.1642099.

[39] S.Y. Heo, S.C. Ko, S.Y. Nam, et al., Fish bone peptide promotes osteogenic differentiation of MC3T3-E1 pre-osteoblasts through upregulation of MAPKs and Smad pathways activated BMP-2 receptor, Cell Biochemistry and Function. 36 (2018) 137-146. https://doi.org/10.1002/cbf.3325.

[40] C. Yan, S.-R. Kim, D.R. Ruiz, et al., Microencapsulation for food applications: A review, ACS Applied Bio Materials. 5 (2022) 5497-5512. https://doi.org/10.1021/acsabm.2c00673.